

# Measurement and Analysis of Real Imaging Systems

František MOJŽIŠ<sup>1</sup>, Jan ŠVIHLÍK<sup>1</sup>, Karel FLIEGEL<sup>2</sup>, Lenka KŇAZOVICKÁ<sup>1</sup>, Eva JERHOTOVÁ<sup>1</sup>

<sup>1</sup>Dept. of Computing and Control Eng., Inst. of Chemical Technology Prague, Technická 5, 166 28 Prague, Czech Republic

<sup>2</sup>Dept. of Radioelectronics, Czech Technical University in Prague, Technická 2, 166 28 Prague, Czech Republic

mojzisz@vscht.cz, svihlikj@vscht.cz, fliegek@fel.cvut.cz, knazovil@vscht.cz, eva.jerhotova@vscht.cz

**Abstract.** *This paper is devoted to statistical analysis of noise generated in real imaging systems and noise suppression methods. The introductory part is focused on description of imaging systems, image degradations, and noise types present in them. The noise analysis section includes determination of basic noise characteristics, the probability distribution and dependence on the signal. The described methods are used to compare properties of two digital still cameras: Nikon D70 and Canon EOS 500D and video camera: JAI CM-040GE. The section devoted to noise suppression discusses different methods of wavelet coefficients thresholding and threshold estimation. The wavelet coefficients are produced by two forms of the wavelet transform: the discrete wavelet transform and the dual-tree complex wavelet transform. The described noise suppression methods are applied to the data sets which were acquired by the analyzed systems under poor lighting conditions.*

## Keywords

Imaging system, noise, statistical analysis, denoising, wavelet transform.

## 1. Introduction

Imaging systems analysis should be a first step before digital image processing [1], [4], [12]. It can give useful information about used system behavior and can give the answer on the question what processing method shall be applied.

This article is devoted to statistical analysis of noise introduced by real imaging systems and brings complex approach to the imaging equipment analysis.

The second aim of this paper is to search a suitable denoising method based on the wavelet coefficients thresholding [8], [12] for the image sets acquired by the systems under analysis during poor lighting conditions. Thorough analysis of this type of system is important for further application of denoising algorithm applied on mentioned type of images. Most common noise present in images is a Gaussian type [1], [4], [12], and denoising methods are well-known for this type of noise. In the described type of images also

noise which is non-Gaussian [1], [4] may be present, therefore denoising methods based on Gaussian thresholding applied on this type of images do not provide satisfactory results. This state is a reason for research of different threshold methods, which can be much more useful and give better results for denoising of images, which are contaminated with non-Gaussian noise.

As mentioned above, the denoising methods based on wavelet coefficients thresholding are usually defined for Gaussian noise. These use simple statistics like median, etc. This paper brings illustration of different techniques of thresholding suitable for non-Gaussian noises. Implementation of these simple methods is based on evaluation of the second central moments using Maximum Likelihood Estimates (MLE). Thus there are used simply implementable methods. The threshold for both mentioned types of noise is optimized on the concrete data and then applied to the real images. Except of MLE, in literature there may also be found threshold estimates based on Bayes estimator.

Two different kinds of wavelet transform [4], [8], [10], [11] are applied for wavelet coefficients evaluation. These are the Discrete Wavelet Transform [4], [8], [10] (DWT) and the Dual Tree Complex Wavelet Transform [11] (DTCWT).

The DWT is probably the most popular wavelet transform. It is computed via the subband coding algorithm introduced by Mallat [8], [10], [14], [15]. At each decomposition level, the analyzed image is decomposed into two types of coefficients: the details and the approximations, which correspond to the upper half and the lower half of the signal spectrum, respectively. The approximations are then used as an input to the next level. The filters used in all decomposition levels create a filter bank [14], [15].

The DTCWT [11] represents a type of the redundant wavelet transform. For two-dimensional signals, this transform produces twice as many coefficients as the DWT. These coefficients are complex and thus composed as a sum of the real ( $c_R$ ) and imaginary ( $c_I$ ) part, i.e.,  $c = c_R + j \cdot c_I$  where  $j = \sqrt{-1}$ .

This article is organized as follows. After description of imaging systems and image distortion in Section 2, approaches to the noise analysis are described in Section 3. Section 4 introduces and compares denoising methods using wavelet coefficients thresholding and finally Section 5

presents noise analysis results of used imaging systems and application of thresholding methods to the data acquired by used cameras.

## 2. Image Distortions

This section describes image degradations, imaging systems, and basic types of noise present in them.

### 2.1 Image Degradations

Generally, images acquired by digital cameras contain noise resulting from digitizing of real patterns. This means that the quality of the final image is influenced by the type and quality of the imaging system, especially by the type of image sensor used in this system. The CCD and CMOS sensors are the two most commonly used types of sensors in these systems. In addition to the sensing elements quality, there are more factors that can influence the resulting image, e.g. degradation due to atmospheric conditions, degradation due to relative motion between the object and the camera, etc.

The degradation process [1], *Gonzalez02* can be described as a degradation function  $h(x,y)$  that together with additive or multiplicative noise  $n(x,y)$  in combination with an input image  $f(x,y)$  produce a degrade image  $g(x,y)$ .

The inverse process, when we want to obtain estimate of the original image, is called restoration. The main purpose of image restoration is to obtain function  $\hat{f}(x,y)$ , which is an estimate of the original image based on some knowledge, usually estimation, of the degradation function  $h(x,y)$  and noise term  $n(x,y)$ .

The image degradation model with additive noise [1], [4] (or signal independent) and model of image degradation with multiplicative noise [1], [4] (or signal dependent) are given by the following relations

$$g(x,y) = h(x,y) * f(x,y) + n(x,y), \quad (1)$$

$$g(x,y) = h(x,y) * f(x,y) \cdot n(x,y) \quad (2)$$

where  $*$  is the convolution operator.

Performance of image sensors used in imaging systems is influenced by a different combination of factors. Firstly, the image can be influenced only by the degradation function ( $n(x,y) = 0$ , Eq. (1), or  $n(x,y) = 1$ , Eq. (2)), secondly, it can be corrupted only by noise ( $h(x,y) = \delta(x,y)$ ), or thirdly, can be given by combination of both noise and degradation function as described by (1) and (2).

### 2.2 Noise in Imaging Systems

Imaging systems consist of many components that form a rather complex structure. A high-level block diagram of the imaging system is shown in Fig. 1.



Fig. 1. Basic block diagram of the imaging system.

Noise reduction constitutes an important problem in applications such as cellular phone communications, image processing, or medical signal processing. The success of a noise reduction method depends on its ability to characterize and model the noise generation process [4], [12].

Noise in digital signals or images [1], [4], [12], [14] can be classified into a few major categories which indicate the physical nature of noise generation. These categories include the thermal noise present in electric conductors, the shot noise generated by the electric current flows, the electromagnetic noise which can interfere with image transmission and reception over the radio-frequency spectrum, the processing noise, and the periodic noise.

Noise in digital images can be described as a statistical quantity. This means that it is a random variable which may be described by its Probability Density Function (PDF) or Probability Mass Function (PMF). The most frequent noise types in digital images, especially in the digital cameras, are Gaussian, Poisson, and Salt and Pepper.

## 3. Noise Analysis

The noise analysis part of this paper discusses basic noise characteristics such as the standard deviation and the Signal to Noise Ratio (*SNR*). Additionally, the Opto-Electronic Conversion Function [5] (*OECF*) as a relationship between input and output values of the imaging system is also evaluated. The applied noise analysis methods are mostly based on the ISO international standards (i.e. ISO 14524 and ISO 15739). The probability distribution of the noise in whole range of the gray scale was tested using image histogram of the analyzed test chart. For this purpose statistical distribution tests were applied. We used the Generalized Laplacian Model (*GLM*) [13], [16] when the statistical tests for other distributions failed.

### 3.1 Basic Noise Measurement

In order to characterize noise in the acquired digital images, we exploit the transmissive chart described by the international standard ISO 15739 [6] (see Fig. 2). In this test chart, patches number 1 to 12 are dedicated to evaluation of the camera *OECF*. Patches number 13 to 15 are designed for measuring noise of different types. Patch 13 is further divided into three sub-patches with different densities [6]. This patch is dedicated to evaluation of basic noise metrics defined by ISO 15739, such as the Signal to Noise Ratio (*SNR*), the noise standard deviation, and the camera dynamic range. Standard deviation may also be applied to the *OECF* patches [5] in order to determine whether the noise is dependent or independent on the underlying signal.

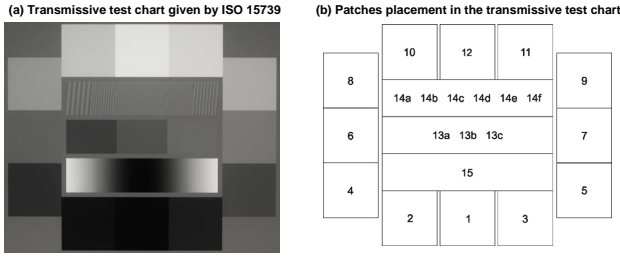


Fig. 2. Noise and OECF measurement test chart and patches placement, (a) Transmissive test chart given by ISO 15739, (b) Patches placement in the transmissive test chart given by ISO 15739.

### Signal to noise ratio

ISO 15739 [6] defines three types of *SNR* characteristics based on the noise type: the total signal to noise ratio ( $SNR_{total}$ ) related to the total noise, the fixed pattern signal to noise ratio ( $SNR_{fp}$ ) related to fixed pattern noise, and the temporal signal to noise ratio ( $SNR_{temp}$ ) related to the temporal noise. The *SNR* can generally be written as

$$SNR_{type} = \frac{L_{sat} \cdot 0.18 \cdot IG}{\sigma_{type}} \quad (3)$$

where  $SNR_{type}$  is related to the corresponding standard deviation ( $\sigma_{type}$ ), i.e. the total ( $\sigma_{total}$ ), the fixed pattern ( $\sigma_{fp}$ ), or the temporal ( $\sigma_{temp}$ ) standard deviation.  $L_{sat}$  denotes the maximum output level of the system, e.g.  $L_{sat} = 255$  for an 8-bit system.  $IG$  represents an incremental gain which is defined as the rate of change in the output level (i.e the digital code value) divided by the rate of change in the input level (luminance or exposure) as a function of the input level [5], [6] and is given by

$$IG = \frac{OL(r_j) - OL(r_i)}{2 \cdot L_{sat}(r_j - r_i)} + \frac{OL(r_k) - OL(r_j)}{2 \cdot L_{sat}(r_k - r_j)} \quad (4)$$

where  $OL(r_j)$  is the digital output signal for patch 13b with the reflectance  $r_j = 0.18$ ,  $OL(r_i)$  is the digital output signal for patch 13a with  $r_i < 0.18$ , and  $OL(r_k)$  is the digital output signal for patch 13c with  $r_k > 0.18$ .

The reflectance is determined from the patch density  $D_i$ . It is also assumed that patch  $j$  has a reflectance of 0.18 assuming a 140 % maximum level, this corresponds to a density 0.9 (patch 13b) with respect to the lightest patch. Reflectance is given by

$$r = 10^{-D_i}. \quad (5)$$

### Fixed pattern noise

The fixed pattern noise [6] is determined by the analysis of the average image which is computed from the acquired data set. The digital code value of a pixel in the average image is given by

$$\bar{g}(x, y) = \frac{1}{n} \sum_{j=1}^n g_j(x, y) = g_{fp}(x, y) + \frac{1}{n} \sum_{j=1}^n g_{temp,j}(x, y) \quad (6)$$

where  $g_j(x, y)$  is the digital code value of a pixel in the corresponding position  $(x, y)$  in the  $j$ -th image and  $g_{temp,j}(x, y)$  is the temporal part of the  $j$ -th image. The variance of the average image is defined as

$$\sigma_{ave}^2 = \sigma_{fp}^2 + \frac{1}{n^2} \sum_{j=1}^n \sigma_{temp,j}^2 = \sigma_{fp}^2 + \frac{1}{n} \sigma_{temp}^2 \quad (7)$$

where  $n$  is number of acquired images,  $\sigma_{fp}$  is the standard deviation of fixed pattern noise and  $\sigma_{temp,j}$  is the standard deviation of the temporally varying part of the  $j$ -th image.

### Temporal noise

The temporal noise [6] is determined by analyzing the difference of an image from the average image. The code values of the difference image are defined as

$$\Delta g_j(x, y) = \left[ \frac{1}{n} \sum_{j=1}^n g_{temp,j}(x, y) \right] - g_{temp,j}(x, y). \quad (8)$$

Then, the overall variance of the code values for the difference image is given by

$$\sigma_{diff}^2 = \frac{1}{n} \sum_{j=1}^n \sigma_{diff,j}^2 = \frac{n-1}{n^2} \sum_{j=1}^n \sigma_{temp,j}^2 = \frac{n-1}{n} \sigma_{temp}^2 \quad (9)$$

where  $\sigma_{diff,j}^2$  is the variance of the code values for the  $j$ -th difference image,  $\sigma_{temp,j}^2$  is the variance of the temporally varying part of the  $j$ -th image, and  $\sigma_{temp}^2$  is the mean of the variances of the temporal noise. The standard deviation of the temporal noise is given by

$$\sigma_{temp} = \sqrt{\frac{n}{n-1} \sigma_{diff}^2}. \quad (10)$$

By using (7) and (10), the standard deviation of the fixed pattern noise is then derived as

$$\sigma_{fp} = \sqrt{\sigma_{ave}^2 - \frac{1}{n-1} \sigma_{diff}^2}. \quad (11)$$

### Total noise

The total noise standard deviation for the  $j$ -th image is given as the square root of the sum of the variances of the temporal noise of the  $j$ -th image and the the fixed pattern noise

$$\sigma_{total,j} = \sqrt{\sigma_{temp,j}^2 + \sigma_{fp}^2}. \quad (12)$$

The overall total noise standard deviation of a measured system is evaluated as the average of all  $\sigma_{total,j}$ .

### Noise type estimation

The noise PDF may be estimated using the Pearson Chi-square test [9], the Kolmogorov-Smirnov test [9], or both, depending on used theoretical distribution. In this paper, we use the Generalized Laplacian Model (GLM) which allows to model different types of the probability density function and can also be used for noise type estimation. The GLM is defined as

$$p(x, s, p) = \frac{e^{-|\frac{x}{s}|^p}}{Z(s, p)} \quad (13)$$

where  $s$  is the bandwidth parameter of the PDF,  $p \in \langle 0.1; 2.5 \rangle$  is the shape parameter, and the function  $Z(s, p)$  is given as

$$Z(s, p) = 2 \frac{s}{p} \Gamma\left(\frac{1}{p}\right). \quad (14)$$

where  $\Gamma(x)$  presents the gamma function.

As shown in [7], [16], the GLM parameters  $s$  and  $p$  may be estimated using the method of moments. Using this method, the second and the fourth central moments are defined as

$$\mu_2(s, p) = \frac{s^2 \Gamma\left(\frac{3}{p}\right)}{\Gamma\left(\frac{1}{p}\right)}, \quad (15)$$

$$\mu_4(s, p) = \frac{s^4 \Gamma\left(\frac{5}{p}\right)}{\Gamma\left(\frac{1}{p}\right)}. \quad (16)$$

By introducing the kurtosis [7], [16], the solution of the above set of equations can be simplified into

$$\hat{\kappa} = \frac{\mu_4(s, p)}{\mu_2^2(s, p)} = \frac{\Gamma\left(\frac{5}{p}\right) \Gamma\left(\frac{1}{p}\right)}{\Gamma^2\left(\frac{3}{p}\right)}. \quad (17)$$

By exploiting this equation, the kurtosis is evaluated for all values of  $p \in \langle 0.1; 2.5 \rangle$  with a chosen  $\Delta p$ . The value of  $\hat{\kappa}$  which falls closest to the kurtosis evaluated for the measured data  $X$  produces the best estimate of the parameter  $p$ . For the normal distribution  $p$  is close to value of 2. The bandwidth parameter  $s$  is then computed from (15)

$$s = \sqrt{\frac{\mu_2\left(\frac{1}{p}\right)}{\mu_2\left(\frac{3}{p}\right)}}. \quad (18)$$

### 3.2 OECF Determination

The OECF is introduced in ISO 14524 [5] and is defined as a relationship between the logarithm of input levels (luminance) and corresponding digital output levels for all OECF patches in the test chart. This information is required for the developments and testing of digital cameras and may be helpful in the digital image processing.

Preferred method for measuring the chart luminance is to use a telescopic photometer. If the transmissive test chart is used, then the luminance  $L_i$  is evaluated as

$$L_i = 10^{-D_i} L, \quad (19)$$

where  $L$  ( $\text{cd}\cdot\text{m}^{-2}$ ) is luminance of the diffuse illuminator on which the test chart is placed. For OECF determination from acquired images, it is necessary to calculate the mean digital output value for each patch. The OECF is then determined either as input  $\log_{10}$  luminance for all test chart patches and the corresponding digital code values, or as  $\log_2$  of the digital code values for each color channel.

## 4. Wavelet Domain Denoising Methods

The noise reduction part of this paper is dedicated to denoising methods and their applications. All the described and applied methods are based on wavelet coefficients thresholding. These coefficients are obtained by exploiting two different forms of the wavelet transform: DWT and DTCWT. In case of the DWT, we use the MAD-based (Median Absolute Deviation) threshold estimate [8], [10] or the GLM-based threshold estimate [7], [16] when the noise is not normally distributed. In case of the DTCWT, we use the threshold estimate based on the Rayleigh distribution [4].

### 4.1 Wavelet Coefficient Thresholding

Denoising methods in the wavelet domain are based on thresholding [8], [12] of the wavelet coefficients obtained by the DWT or the DTCWT of the original image. The thresholding algorithms [8], [12] are applied to high-frequency coefficients (the details). The denoised image is then obtained by the inverse wavelet transform [4], [8], [10], [11].

The threshold value is usually estimated from the high-frequency content of the given signal. Then we are able to apply the thresholding functions (algorithms), such as hard and soft, which are given by the following equations

$$y_{\text{hard}}(i) = \begin{cases} x(i) & \text{for } |x(i)| > \gamma, \\ 0 & \text{for } |x(i)| \leq \gamma, \end{cases} \quad (20)$$

$$y_{\text{soft}}(i) = \begin{cases} \text{sign}(x(i))(|x(i)| - \gamma) & \text{for } |x(i)| > \gamma, \\ 0 & \text{for } |x(i)| \leq \gamma \end{cases} \quad (21)$$

where  $x(i)$  are input signal values and  $\gamma$  is the threshold.

In case of the DTCWT, we threshold only magnitudes of the complex coefficients and keep the phase  $\angle x(i)$  unchanged [11]. The thresholded coefficients are then given as

$$y_{\text{thr}}(i) = |x(i)| e^{j\angle x(i)} \quad (22)$$

where the magnitude  $|x(i)|$  was thresholded either by Eq. (20) or (21).

The experimental results of different thresholding methods are compared using the Root Mean Square Error (RMSE) measure.

### 4.2 Threshold Estimation

Threshold estimation algorithms are based on evaluation of the noise standard deviation  $\hat{\sigma}$ . This relationship can be generally written as

$$\gamma_{\text{general}} = \hat{\sigma} \xi. \quad (23)$$

The constant  $\xi$  may be evaluated experimentally as

$$\xi = \arg \min_{\xi} RMSE(\hat{f}(x, y), \bar{g}(x, y)) \quad (24)$$

where  $\hat{f}(x,y)$  represents the best estimate of the restored image and  $\bar{g}(x,y)$  is the average image. Alternatively, the constant  $\xi$  may be derived by optimization. A well known method is the universal threshold [2]

$$\gamma_{UNIV} = \hat{\sigma}\sqrt{2\ln n} \quad (25)$$

where  $n$  is the analyzed signal length,  $\hat{\sigma}$  is the estimate of the standard deviation of the additive Gaussian noise. Another method used for threshold value estimation is the SURE algorithm [3] (Stein's Unbiased Estimate of Risk) defined as

$$\gamma_{SURE} = \hat{\sigma}\sqrt{2\ln\left(n\frac{\ln n}{\ln 2}\right)}. \quad (26)$$

The standard deviation of the additive noise can be estimated by exploiting the MAD

$$\hat{\sigma}_{MAD} = \frac{\text{median}\{|c_D|\}}{0.6745} \quad (27)$$

or the Maximum Likelihood in the Wavelet Domain (MLWD) algorithm

$$\hat{\sigma}_{MLWD} = \sqrt{\frac{1}{n}\sum_{i=1}^n (c_{D,i} - \bar{c}_D)^2} \quad (28)$$

where  $c_D$  is a vector of the wavelet coefficients presenting the high frequency components of the analyzed signal,  $\bar{c}_D$  is its mean, and  $c_{D,i}$  are the individual coefficients. It is important to mention that the MLWD estimate is not so robust as the MAD estimate.

The above described methods of  $\sigma$  estimation are based on the fact that the noise distribution is normal. A more general method of threshold determination can be derived from the GLM model. If we define the standard deviation as the square root of the variance and if the variance is replaced by the estimate of the second central moment  $\mu_2$  of the GLM, then the threshold value estimate  $\gamma$  may be derived as

$$\gamma = \xi\sqrt{\mu_2(s,p)} = \xi\sqrt{\frac{s^2\Gamma\left(\frac{3}{p}\right)}{\Gamma\left(\frac{1}{p}\right)}}. \quad (29)$$

In case of the complex coefficients produced by the DTCWT we preserve the original phase and threshold only magnitudes, (22). This leads to the conclusion, that the probability distribution function of the wavelet coefficients magnitude is asymmetric. When we assume that the real and imaginary parts are normally distributed, the magnitude is then Rayleigh distributed [11]

$$p(x,\sigma) = \frac{x}{\sigma^2}e^{-\frac{x^2}{2\sigma^2}} \quad (30)$$

where  $x \geq 0$  and  $\sigma > 0$ . The threshold value is then defined as

$$\gamma = \xi\sqrt{\mu_2(\sigma)} = \xi\sqrt{2\sigma^2\Gamma(2)} \quad (31)$$

and its parameter  $\sigma$  may be estimated by the maximum likelihood method [7], [11]

$$\hat{\sigma} = \sqrt{\frac{1}{2I}\sum_{i=1}^I |N(i)|^2} \quad (32)$$

where  $N$  are the complex wavelet coefficients of noise.

Depending on the approach of  $\hat{\sigma}$  evaluation we speak either about a global threshold, for which  $\hat{\sigma}$  is estimated only at the first level of wavelet decomposition, e.g. MAD estimate, and the same threshold value is applied to all detail coefficients subbands, or a local threshold, for which the threshold value is determined separately for each subband, e.g., GLM estimate.

## 5. Results

In this section there are presented results of approaches described in the previous sections that were applied to the data acquired by uses cameras. Tab. 1 shows basic properties of the three analyzed imaging systems.

camera	Nikon D70	Canon EOS 500D	JAI CM-040GE
description	SLR camera	SLR camera	video camera
sensor type	CCD	CMOS	CCD
sensor resolution	6.1 mil. of px.	15.1 mil. of px.	0.45 mil. of px.
ISO sensitivity	200 - 1600	100 - 6400	undefined
used compression	none	none	none

Tab. 1. Basic properties of analyzed imaging systems.

### 5.1 Noise Analysis Results

Figs. 3, 4, and 5 present examples of the evaluated OECF values of the analyzed imaging systems for a chosen ISO sensitivity.

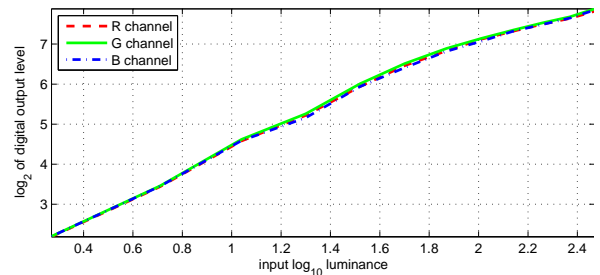


Fig. 3. Nikon D70 OECF, ISO-200, log<sub>2</sub> of digital output level vs. input log<sub>10</sub> luminance.

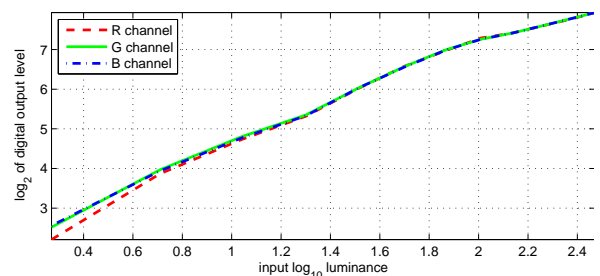


Fig. 4. Canon EOS 500D OECF, ISO-200, log<sub>2</sub> of digital output level vs. input log<sub>10</sub> luminance.

It can be observed that the OECF curves of all the analyzed systems are non-linear. The evaluated noise standard deviations of Nikon D70 and Canon EOS 500D for all ISO sensitivities are presented in Fig. 6. The values of  $\sigma_{total}$  for JAI CM-040GE is 2.88. Fig. 7 contains  $SNR_{total}$  of both digital still cameras. The value of  $SNR_{total}$  of the CM-040GE camera is 33.98. Figs. 8, 9 and 10 show trends of  $\sigma_{total}$  in the OECF patches. Based on the result of the noise analysis for the OECF patches it can be said that the noise is weakly signal dependent.

Figs. 11 and 12 present histograms for the OECF patches of all the analyzed systems for the chosen ISO sensitivity. These histograms were used for estimating the noise probability distribution. The normal, Poisson, Erlang, Rayleigh, and exponential distributions were tested.

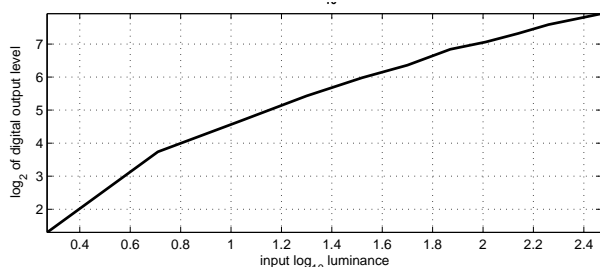


Fig. 5. CM-040GE OECF,  $\log_2$  of digital output level vs. input  $\log_{10}$  luminance.

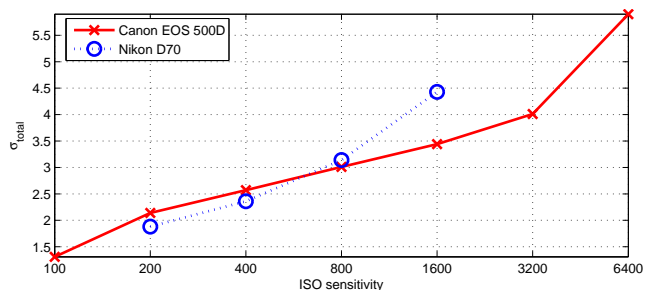


Fig. 6. Total standard deviations of Nikon D70 and Canon EOS 500D vs. ISO sensitivity.

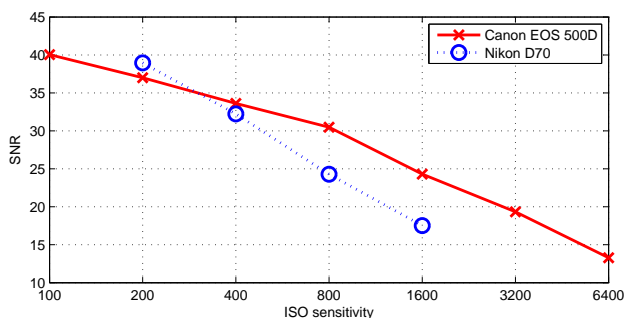


Fig. 7.  $SNR_{total}$  of Nikon D70 and Canon EOS 500D vs. ISO sensitivity.

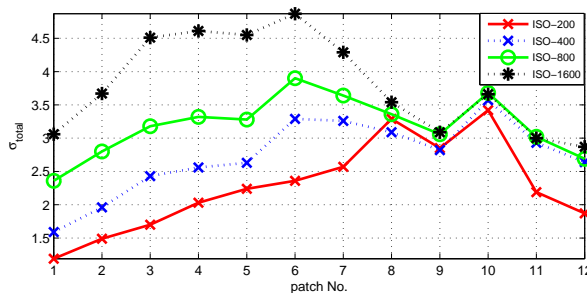


Fig. 8. Nikon D70,  $\sigma_{total}$  in OECF patches for chosen ISO.

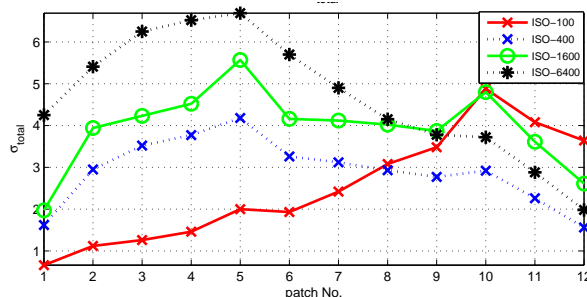


Fig. 9. Canon EOS 500D,  $\sigma_{total}$  in OECF patches for chosen ISO.

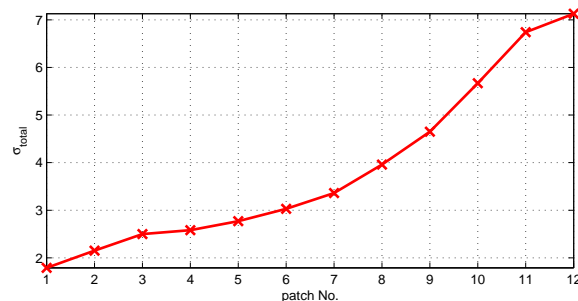


Fig. 10. JAI CM-040GE,  $\sigma_{total}$  in OECF patches.

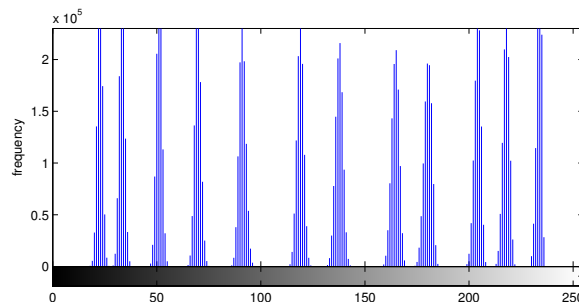


Fig. 11. Nikon D70, histogram of OECF patches, ISO-200.

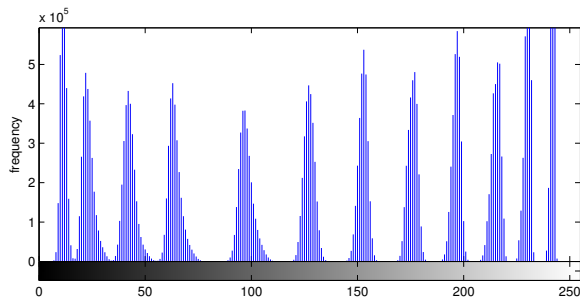


Fig. 12. Canon EOS 500D, histogram of OECF patches, ISO-800.

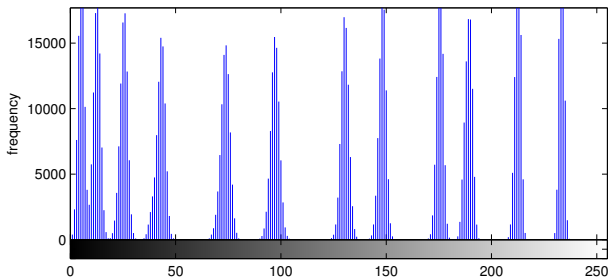


Fig. 13. JAI CM-040GE, histogram of OECF patches.

The Kolmogorov-Smirnov and the  $\chi^2$  test of goodness of fit rejected the null hypothesis for all the tested distributions at the significance level  $\alpha = 0.05$ . Hence the shape parameter  $p$  of the GLM model was used for noise type estimation as shown in Figs. 14, 15, and 16. Since  $p$  is different from value of 2 in a majority of patches (the OECF patches in particular), the noise cannot be considered normally distributed.

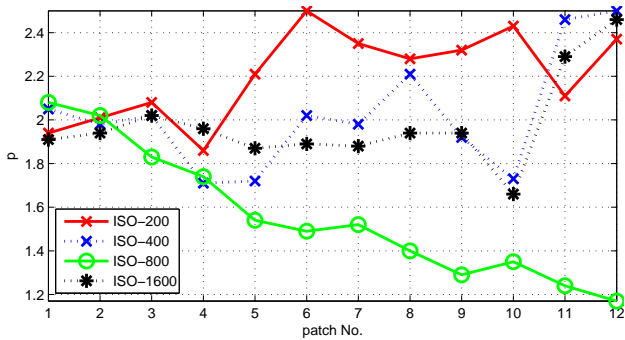


Fig. 14. Nikon D70, GLM shape parameter in OECF patches.

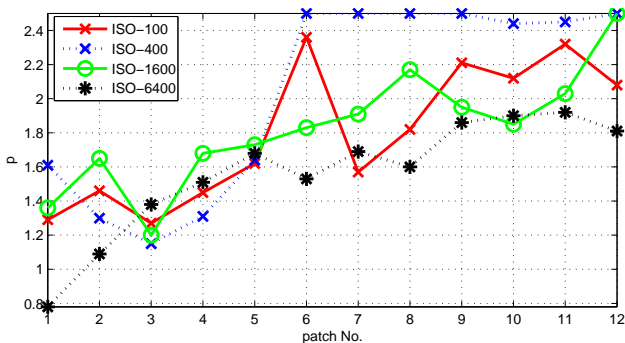


Fig. 15. Canon EOS 500D, GLM shape parameter in OECF patches.

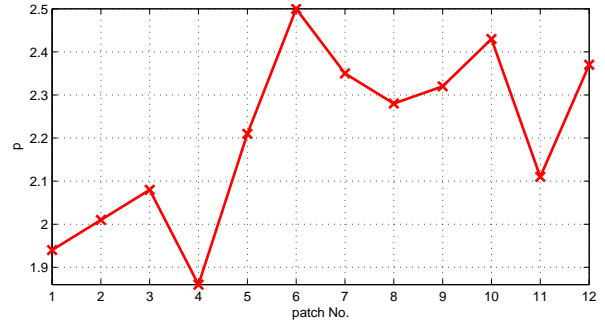


Fig. 16. JAI CM-040GE, GLM shape parameter in OECF patches.

### 5.2 Denoising Methods Application

The denoising methods were applied to the acquired sets (of 8 images for each camera) with the same ISO sensitivity settings as we used for the noise analysis. The average image for each set was computed and  $RMSE_j$  of the  $j$ -th image was evaluated. The overall  $RMSE$  is given as the mean of all  $RMSE_j$  and represents the given data set and we compare its value before and after denoising.

Local threshold estimate based on the MAD and the GLM approaches in combination with hard and soft thresholding were used for denoising in the wavelet domain (both applying the DWT and the DTCWT).

#### Nikon D70

For visual evaluation of the denoising results, a cut of a selected image acquired by Nikon D70 with ISO 1600, and the average image of the corresponding data set are displayed in Fig. 17 and 18.

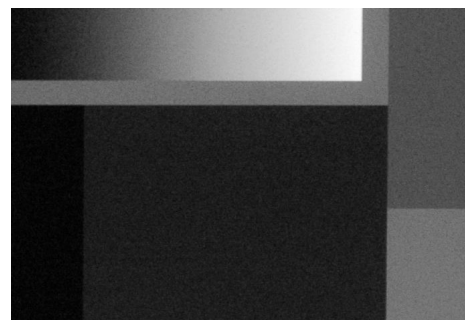


Fig. 17. Nikon D70 ISO-1600 - cut of selected image number 4.

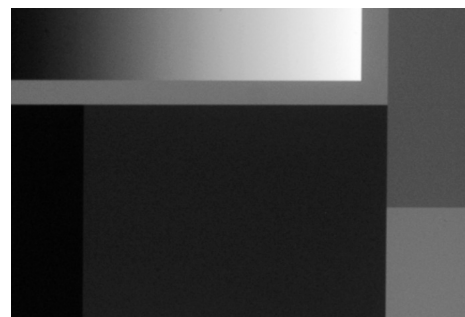


Fig. 18. Nikon D70 ISO-1600 - cut of average image.

Tab. 2 contains values of the noisy *RMSE* for the used ISO sensitivities and Fig. 19 presents trend of the *RMSE* measure in the original data set and the resulting *RMSE* after denoising for each applied ISO sensitivity. Detailed results can be seen in Tabs. 3 and 4 which comprise the *RMSE* values after thresholding the DWT and the DTCWT coefficients, respectively.

ISO	200	400	800	1600
RMSE	2.4232	2.1722	3.6727	3.6307

Tab. 2. Nikon D70 - noisy *RMSE* values for given ISO.

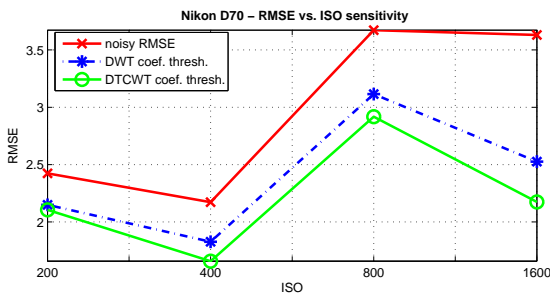


Fig. 19. Nikon D70 - noisy *RMSE* and *RMSE* after wavelet coefficients thresholding vs. ISO sensitivity.

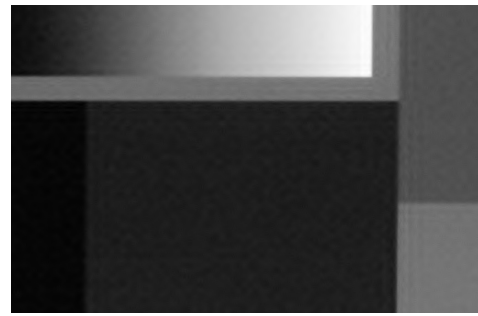


Fig. 20. Nikon D70 ISO-1600 - cut of thresholded image no. 4 denoised using DWT, 3<sup>rd</sup> dec. level, soft thr.,  $\gamma_{\text{EXPM}}$ ,  $\hat{\sigma}_{\text{MAD}}$ .

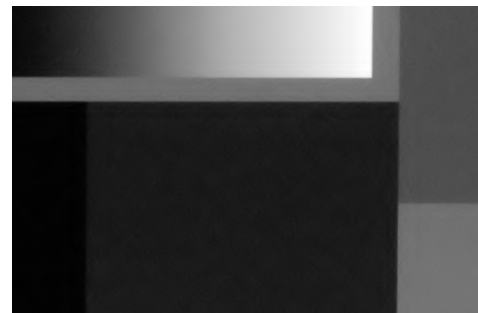


Fig. 21. Nikon D70 ISO-1600 - cut of thresholded image no. 4 denoised using DTCWT, 4<sup>th</sup> dec. level, soft thr.,  $\gamma_{\text{EXPM}}$ .

ISO	$\gamma$	MAD $\sigma$ estimate			GLM $\sigma$ estimate		
		dec. level	threshold		dec. level	threshold	
			hard	soft		hard	soft
200	UNIV	3	2.2763	2.1541	3	2.2855	2.1820
	SURE	3	2.2742	2.1601	3	2.2874	2.1822
	EXPM	3	2.2813	2.1496	3	2.2854	2.1778
400	UNIV	3	1.8616	1.8605	3	1.8946	1.8595
	SURE	3	1.8596	1.8479	3	1.9032	1.8719
	EXPM	4	1.8651	1.8272	3	1.8916	1.8470
800	UNIV	4	3.2066	3.1454	3	3.2602	3.2248
	SURE	4	3.2002	3.1755	3	3.2709	3.2357
	EXPM	4	3.2248	3.1145	3	3.2546	3.2136
1600	UNIV	4	2.7440	2.5636	3	2.7911	2.7424
	SURE	4	2.7132	2.6003	3	2.7910	2.7734
	EXPM	4	2.8016	2.5264	3	2.8058	2.6854

Tab. 3. Nikon D70 - *RMSE* after thresholding of wavelet coefficients obtained by DWT.

ISO	dec. level	threshold	
		hard	soft
200	3	2.2189	2.1059
400	4	1.7018	1.6584
800	4	2.9625	2.9177
1600	4	2.2119	2.1742

Tab. 4. Nikon D70 - *RMSE* after thresholding of complex wavelet coefficients obtained by DTCWT.

It is obvious that the difference between the *RMSE* gained by the DTCWT and the DWT increases with the increasing ISO sensitivity. The *RMSE* results also suggest that the DTCWT gives better results than the DWT, especially for higher ISO sensitivities. This is also visible on the cuts of the restored images in Figs. 20 and 21 as the DTCWT surpasses the DWT in preserving image edges.

### Canon EOS 500D

Figs. 22 and 23 present respectively a cut of a selected image and a cut of the average image for the data set acquired by Canon EOS 500D.

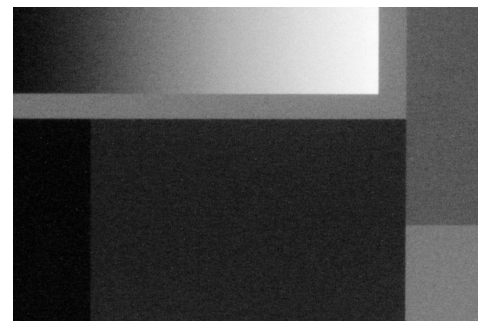


Fig. 22. Canon EOS 500D ISO-6400 - cut of image no. 4.

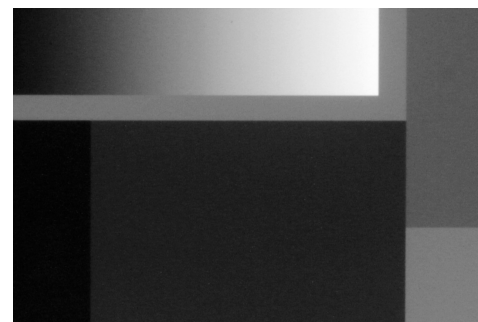


Fig. 23. Canon EOS 500D ISO-6400 - cut of average image.

Tab. 5 contains the noisy *RMSE* values for the used ISO sensitivities. Fig. 24 contains the *RMSE* characteristic of processed data before and after wavelet coefficients thresholding for each ISO sensitivity value. Also for this camera, the difference between the *RMSE* resulting from the DTCWT coefficients thresholding and the DWT coefficients thresholding gradually increases. Tabs. 6 and 7 display the detailed denoising results.

ISO	100	200	400	800	1600	3200	6400
RMSE	0.6739	0.8815	1.1277	1.4801	1.9136	2.7026	4.1593

Tab. 5. Canon EOS 500D - noisy *RMSE* values for given ISO sensitivity.

Fig. 25 and 26 depict crops of the resulting denoised images and again the result obtained using the DTCWT is visually better.

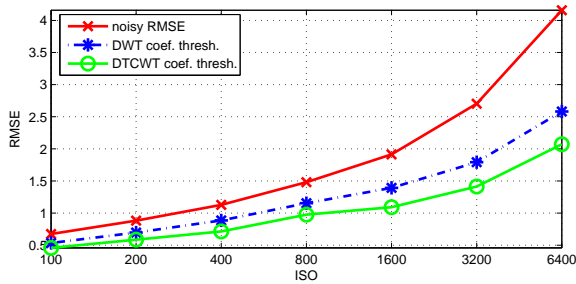


Fig. 24. Canon EOS 500D - noisy *RMSE* and *RMSE* after wavelet coefficients thresholding vs. ISO sensitivity.

ISO	$\gamma$	MAD $\sigma$ estimate				GLM $\sigma$ estimate			
		dec. level	threshold		dec. level	threshold			
			hard	soft		hard	soft		
100	UNIV	3	0.5584	0.5597	3	0.5619	0.6095		
	SURE	4	0.5338	0.5692	3	0.5687	0.5928		
	EXPM	4	0.5445	0.5470	3	0.5722	0.5961		
200	UNIV	4	0.6973	0.7625	4	0.7265	0.8180		
	SURE	4	0.6977	0.7683	3	0.7350	0.7813		
	EXPM	4	0.7037	0.7359	3	0.7196	0.7689		
400	UNIV	4	0.8863	0.9543	4	0.9099	1.0335		
	SURE	4	0.8845	0.9619	3	0.9202	0.9819		
	EXPM	4	0.8988	0.9186	3	0.9034	0.9627		
800	UNIV	4	1.1703	1.1832	3	1.1925	1.2392		
	SURE	4	1.1623	1.2051	3	1.2008	1.2443		
	EXPM	4	1.1936	1.1537	3	1.1906	1.2322		
1600	UNIV	3	1.4148	1.4336	3	1.4287	1.5185		
	SURE	4	1.4002	1.4638	3	1.4402	1.5250		
	EXPM	3	1.4548	1.3925	4	1.4299	1.4888		
3200	UNIV	4	1.9042	1.8268	3	1.9213	1.9701		
	SURE	4	1.8720	1.8525	3	1.9364	2.0058		
	EXPM	3	1.9797	1.7925	4	1.9231	1.9178		
6400	UNIV	4	2.8479	2.6121	4	2.8224	2.7014		
	SURE	4	2.7909	2.6275	4	2.8297	2.7164		
	EXPM	4	2.9762	2.5821	4	2.8422	2.6770		

Tab. 6. Canon EOS 500D - *RMSE* after thresholding of DWT coefficients.

ISO	dec. level	threshold	
		hard	soft
100	4	0.4597	0.4587
200	4	0.5889	0.5855
400	4	0.7211	0.7139
800	4	0.9941	0.9756
1600	4	1.0922	1.0905
3200	4	1.4140	1.4126
6400	4	2.0962	2.0717

Tab. 7. Canon EOS 500D - *RMSE* after thresholding of DTCWT coefficients.

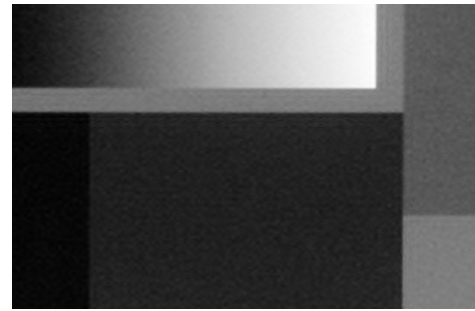


Fig. 25. Canon EOS 500D ISO-6400 - cut of thresholded image no. 4 denoised using DWT, 3<sup>rd</sup> dec. level, soft thr.,  $\gamma_{EXPM}$ , MAD  $\sigma$  estimate.

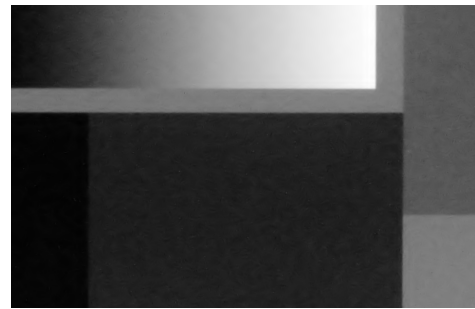


Fig. 26. Canon EOS 500D ISO-6400 - cut of thresholded image no. 4 denoised using DTCWT, 4<sup>th</sup> dec. level, soft thr.,  $\gamma_{EXPM}$ .

JAI CM-040GE

Figs. 27 and 28 show respectively a cut of a selected image and a cut of the average image for the data set acquired by the JAI CM-040GE camera.

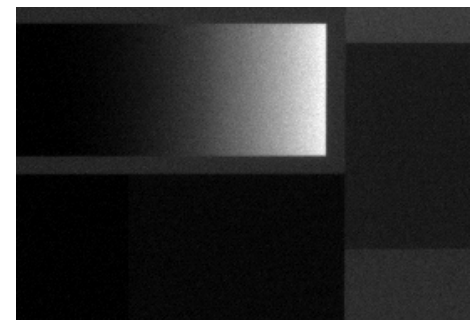


Fig. 27. JAI CM-040GE - cut of image no. 4.



Fig. 28. JAI CM-040GE - cut of average image.

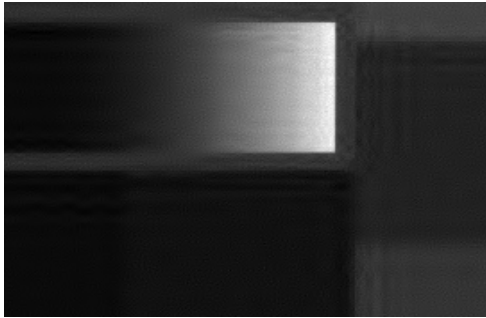


Fig. 29. JAI CM-040GE - cut of thresholded image no. 4 denoised using DTCWT, 3<sup>rd</sup> dec. level, hard thr.,  $\gamma_{SURE}$ , MAD  $\sigma$  estimate.

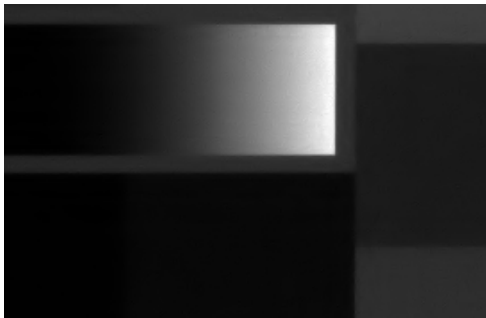


Fig. 30. JAI CM-040GE - cut of thresholded image no. 4 denoised using DTCWT, 4<sup>th</sup> dec. level, soft thr.,  $\gamma_{EXPM}$ .

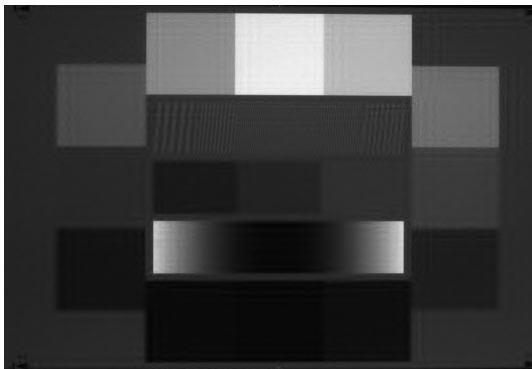


Fig. 31. JAI CM-040GE - thresholded image no. 4 denoised using DWT, 3<sup>rd</sup> dec. level, hard thr.,  $\gamma_{SURE}$ , MAD  $\sigma$  estimate.

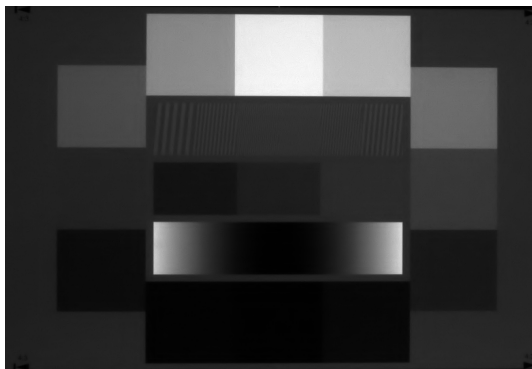


Fig. 32. JAI CM-040GE - thresholded image no. 4 denoised using DTCWT, 4<sup>th</sup> dec. level, soft thr.,  $\gamma_{EXPM}$ .

Tabs. 8 and 9 contain the *RMSE* results. The noisy *RMSE* value for this camera was 2.9837.

$\gamma$	MAD $\sigma$ estimate			GLM $\sigma$ estimate		
	dec. level	threshold		dec. level	threshold	
		hard	soft		hard	soft
UNIV	3	1.5447	1.7028	2	1.6760	2.0352
SURE	3	1.5339	7.7652	2	1.7370	2.1083
EXPM	3	1.5509	1.6908	2	1.6650	2.0206

Tab. 8. JAI CM-040GE - *RMSE* after thresholding of DWT coefficients.

dec. level	threshold	
	hard	soft
4	1.0896	1.2304

Tab. 9. JAI CM-040GE - *RMSE* after thresholding of DTCWT coefficients.

Also for the JAI CM-040GE system, the restored images present considerable potential of the DTCWT in combination with the threshold estimate given by (31) and (32). When we look at edges in Figs. 29 and 31 we can again see that they are largely blurred. Figs. 30 and 32 present the same image and its crop restored after thresholding of the complex wavelet coefficients produced by the DTCWT.

## 6. Conclusion

This paper analyzes three imaging systems: Nikon D70, Canon EOS 500D, and JAI CM-040GE. The OECF curves of these systems reveal nonlinear behavior which represents a rather limiting factor in noise rejection. Another limitation is given by the fact that the noise present in the images acquired in poor lighting conditions is not normally distributed and it is also slightly signal dependent in the whole grayscale range for all the ISO sensitivities.

We also describe and apply wavelet-based denoising methods. The methods are compared by evaluating of the *RMSE* improvement and visual assessment. We may conclude that thresholding of the complex wavelet coefficients obtained from the DTCWT produces better results than thresholding the real coefficients produced by the DWT. The reason might be a more convenient way of signal interpretation in the complex coefficients whose magnitude is shift-invariant. Additionally, the DWT-based method was a little handicapped since the noise in the analyzed systems was not normally distributed, however, we used the MAD method (designed for the normal distribution) for the noise standard deviation estimation.

Wavelet coefficients were adjusted using hard and soft thresholding algorithms. The difference between them are not significant as well as the differences between local and global thresholding. Threshold estimates in case of the DWT were based on MAD and GLM estimates. Rayleigh distribution was applied while using the DTCWT. The estimates based on the Rayleigh distribution gave the best results for all processed images in comparisons to MAD and GLM approaches.

## Acknowledgements

This work has been supported by the research project MSM 6046137306 of the Ministry of Education, Youth and Sports of the Czech Republic and by the Czech Grant Agency under grants No. 205/09/1302 "Study of sporadic meteors and weak meteor showers using automatic video intensifiers cameras", No. P102/10/1320 "Research and modeling of advanced methods of image quality evaluation" and by the research program MSM 6840770014 "Research in the Field of Information and Communication Technology".

## References

- [1] ACHARYA, T., AJOY, K. R. *Image Processing: Principles and Applications*. New York (USA): Wiley, 2005.
- [2] DONOHO, D. L., JOHNSTONE, I. M. Ideal spatial adaptation by wavelet shrinkage. *Biometrika*, 1994, vol. 81, no. 3, p. 425 - 455.
- [3] DONOHO, D. L., JOHNSTONE, I. M. Adapting to unknown smoothness via wavelet shrinkage. *Journal of the American Statistical Association*, 1994, vol. 90, no. 432, p. 1200 - 1224.
- [4] GONZALEZ, C. R., WOODS, E. R.: *Digital Image Processing*. 2<sup>nd</sup> ed. Upper Saddle River (NJ, USA): Prentice Hall, 2002.
- [5] *International standard ISO 14524:1999(E)*. ISO copyright office, 1999.
- [6] *International standard ISO 15739:2003(E)*. ISO copyright office, 2003.
- [7] JERHOTOVÁ, E., ŠVIHLÍK, J., PROCHÁZKA, A. Biomedical image volumes denoising via the wavelet transform. *Applied Biomedical Engineering*. Rijeka (Croatia): InTech, 2011, p. 435 - 458.
- [8] KINGSBURY, N. G. *4F8 Image Coding Course*. Berlin (Germany): Springer, 2006.
- [9] PAVLÍK, J. *et al. Applied statistics*. ICT, 2005. In Czech.
- [10] PERCIVAL, D. B., WALDEN, A. T. *Wavelet Methods for Time Series Analysis*. 2<sup>nd</sup> ed. Cambridge (UK): Cambridge University Press, 2006.
- [11] SELENICK, W., BARANIUK, R. G., KINGSBURY, N. G. The dual-tree complex wavelet transform. *IEEE Signal Processing Magazine*, 2005, vol. 22, no. 6, p. 123 - 151.
- [12] VASEGHI, S. V. *Advanced Digital Signal Processing and Noise Reduction*. 3<sup>rd</sup> ed. New York: Wiley, 2006.
- [13] SIMONCELLI, E. P., ADELSON, E. H. Noise removal via Bayesian wavelet coring. In *International Conference on Image Processing (ICIP-96)*. Lausanne (Switzerland), 1996, vol. I, p. 379 - 382.
- [14] STARCK, J. L., MURTAGH, F., BIAOUI, A. *Image Processing and Data Analysis: The Multiscale Approach*. Cambridge (UK): Cambridge University Press, 1998.
- [15] STRANG, G., NGUYEN, T. *Wavelets and Filter Banks*. 2<sup>nd</sup> ed. Wellesley (MA, USA): Wellesley-Cambridge Press, 1996.
- [16] ŠVIHLÍK, J., FLIEGEL, K., KOTEN, P., VÍTEK, S., PÁTA, P. Noise analysis of MAIA system and possible noise suppression. *Radioengineering*, 2011, vol. 20, no. 1, p. 110 - 117.
- [17] TUKEY, J. W. *Exploratory Data Analysis*. Boston (MA, USA): Addison Wesley, 1977.
- [18] PRESS, W. H., TEUKOLSKY, S. A., VETTERLING, W. T., FLANNERY, B. P. *Numerical Recipes: The Art of Scientific Computing*. 3<sup>rd</sup> ed. Cambridge (UK): Cambridge University Press, 2007.

## About Authors...

**František MOJŽIŠ** was born in Prague, Czech Republic in 1986. He received his M.Sc. from the Institute of Chemical Technology Prague (ICT), in 2011. Now he is a Ph.D. student at ICT. His research interests include image processing and image denoising.

**Jan ŠVIHLÍK** was born in Pardubice, Czech Republic, in 1981. He received his M.Sc. from the Czech Technical University in Prague (CTU) in 2005 and Ph.D. from the CTU, in 2008. Now he is an Assistant Professor at the Institute of Chemical Technology Prague. His research interests include image processing, image denoising and statistical models of images.

**Karel FLIEGEL** was born in Prague, Czech Republic, in 1979. He received his M.Sc. degree in electrical engineering from the Czech Technical University in Prague (CTU) in 2004 and Ph.D. from the CTU in 2011. Now he is an Assistant Professor at the CTU. His research interests include image processing, imaging systems, image and video compression.